HHS Public Access

Author manuscript

Biochem J. Author manuscript; available in PMC 2022 September 18.

Published in final edited form as:

Biochem J. 2021 August 13; 478(15): 2999–3014. doi:10.1042/BCJ20210378.

PARP7 mono-ADP-ribosylates the Agonist Conformation of the Androgen Receptor in the Nucleus

Teddy Kamata,

Chun-Song Yang,

Bryce M. Paschal*

Department of Biochemistry and Molecular Genetics, University of Virginia School of Medicine, Charlottesville, VA 22908, USA

Abstract

We recently described a signal transduction pathway that contributes to androgen receptor (AR) regulation based on site-specific ADP-ribosylation by PARP7, a mono-ADP-ribosyltransferase implicated in several human cancers. ADP-ribosylated AR is recognized by PARP9/DTX3L, a heterodimeric complex that contains an ADP-ribose reader (PARP9) and a ubiquitin E3 ligase (DTX3L). Here, we have characterized the cellular and biochemical requirements for AR ADP-ribosylation by PARP7. We found that the reaction requires nuclear localization of PARP7 and an agonist-induced conformation of AR. PARP7 contains a Cys_3His_1-type zinc finger (ZF), which also is critical for AR ADP-ribosylation. The Parp7 ZF is required for efficient nuclear import by a nuclear localization signal (NLS) encoded in PARP7, but rescue experiments indicate the ZF makes a contribution to AR ADP-ribosylation that is separable from the effect on nuclear transport. ZF mutations do not detectably reduce PARP7 catalytic activity and binding to AR, but they do result in the loss of PARP7 enhancement of AR-dependent transcription of the *MYBPC1* gene. Our data reveals critical roles for AR conformation and the PARP7 ZF in AR ADP-ribosylation and AR-dependent transcription.

Introduction

More than 1.2 million men in the world were diagnosed with prostate cancer (PCa) in 2018, making it the second most frequently diagnosed cancer in men and a disease that contributes significantly to healthcare costs [1]. Many studies point to signaling and gene expression mediated by the androgen receptor (AR) as a primary driver of PCa. AR is a member of the nuclear receptor superfamily of ligand-activated transcription factors that upon binding

***Corresponding Author Contact Information**: Bryce M. Paschal, Professor of Biochemistry and Molecular Genetics, University of Virginia, Room 7021 West Complex, Box 800577, Charlottesville, VA 22908, Tel (434) 243 6521, paschal@virginia.edu.

Author Contributions

BMP: Conceptualization, Supervision, Funding acquisition, Methodology, Project administration, Writing — review and editing. TK: Conceptualization, Formal analysis, Validation, Investigation, Visualization, Methodology, Writing — original draft, Writing — review and editing. CY: Conceptualization, Validation, Investigation, Writing — review and editing.

Data Availability Statement Source data available upon request.

Competing Interests Statement

The authors declare no competing interests associated with the study.

androgen adopts an agonist conformation which is active for transcriptional regulation [2,3]. A mainstay of PCa treatment is androgen deprivation therapy (ADT), the goal of which is to inhibit AR signaling by blocking androgen synthesis and/or preventing androgen from binding to AR with anti-androgens which induce an antagonist, inactive conformation of AR [4]. ADT generally achieves positive responses in PCa patients; however, disease relapse can occur as a result of reactivation of AR signaling pathway [5,6]. The failure of current therapies to manage PCa emphasizes the need to better understand the regulatory mechanisms that control AR activity.

Our lab recently described a novel signal transduction pathway that modulates AR activity through ADP-ribosylation [7]. The pathway is dependent on the mono-ADP-ribosyltransferase PARP7. The other names for this enzyme include 2,3,7,8-tetrachlorodibenzo-*p*-dioxin-inducible poly-ADP-ribose polymerase (TIPARP) and ADP-ribosyltransferase diphtheria toxin-like 14 (ARTD14). *PARP7* is a direct AR target gene and in PCa cells can be induced >10-fold by androgen [7,8]. Androgen treatment also promotes PARP7 protein stability through a mechanism that is AR-dependent but independent of *PARP7* transcription [9]. The sum of these two mechanisms drives PARP7 expression, which, in turn, mediates cysteine ADP-ribosylation of AR [7]. Cysteine ADP-ribosylation on AR creates binding sites for PARP9 (mono-ADP-ribosyltransferase)/DTX3L (E3 ubiquitin ligase) heterodimer [7]. Highly specific recognition of the ADP-ribose moiety by tandem macrodomains within PARP9 result in recruitment of the PARP9/DTX3L complex to ADP-ribosylated AR. AR-PARP9/DTX3L complex assembly serves to help regulate the transcriptional output from a subset of AR-target genes in PCa cells. Thus, PARP7 provides an additional layer of regulation for AR-dependent transcription.

Here, we have characterized AR ADP-ribosylation mediated by PARP7 and show that the reaction is highly dependent on AR adopting an agonist conformation. We found that nuclear import of PARP7 is critical for AR ADP-ribosylation, consistent with the reaction occurring within the nucleus. Our structure-function analysis showed that the Cys_3His_1-type zinc finger (ZF) domain in PARP7 modulates PARP7 import, but the PARP7 ZF also plays a transport-independent role in AR ADP-ribosylation that is important for AR-dependent transcription.

Results

An agonist conformation of AR is required for ADP-ribosylation by PARP7

In previous work, we showed that androgen regulates AR ADP-ribosylation through two distinct mechanisms that contribute to PARP7 expression: androgen induction of *PARP7* transcription [7] and androgen induction of PARP7 protein stability [9]. Both mechanisms are critical for determining the cellular concentration of PARP7. Given that androgen induces conformational changes in AR, in the current study we queried whether androgen binding might also contribute to AR ADP-ribosylation by modulating protein structure in a manner that enhances AR suitability as a substrate for PARP7. A precedent for androgen regulation of AR as a substrate comes from studies showing that androgen binding to the C-terminal ligand binding domain (LBD) induces multi-site serine phosphorylation in the N-terminal domain of AR [10].

To address the question of whether androgen binding to AR induces a structure that is critical for ADP-ribosylation, we took advantage of AR LBD mutants that were discovered in patients, have been characterized biochemically, and map to helix 10/11 of the LBD (Figure 1A). The L860F substitution was identified in a patient with complete androgen insensitivity syndrome and reduces androgen binding to ~14% of WT [11]. The T878A mutation commonly found as a resistance mechanism in PCa patients undergoing ADT broadens the ligand specificity of the LBD and enables the androgen antagonist hydroxyflutamide (HO-Flutamide) to induce an agonist conformation in AR [12–14]. By design, the assays were performed in AR-negative HEK293T cells to avoid the confounding effects of AR and PARP7 gene induction in PCa cell lines.

HEK293T cells were transiently transfected with HA-PARP7, alone, and in combination with Flag-AR WT and Flag-AR L860F (Figure 1B). After cell treatment with R1881 (synthetic androgen) and vehicle, AR was immunoprecipitated and probed for ADP-ribosylation using fluorescently labeled AF1521 [9]. Co-expression of HA-PARP7 and Flag-AR WT was not sufficient for AR ADP-ribosylation unless androgen was added to the cells (Figure 1B, lanes 2 and 3). This shows that androgen is still required for AR ADP-ribosylation even if PARP7 is provided by ectopic expression. When the same assay was performed using the Flag-AR L860F mutant, ~10-fold less AR ADP-ribosylation was observed in the presence of androgen as compared to Flag-AR WT (Figure 1B, lane 5). These data show that androgen binding to the LBD, which induces an agonist conformation in AR, is a prerequisite for ADP-ribosylation by PARP7. To compare PARP7 ADP-ribosylation of ligand-free, agonist-bound, and antagonist-bound forms of AR, we transfected cells with HA-PARP7 and Flag-AR WT, and treated cells with R1881 (agonist) and anti-androgen HO-Flutamide (antagonist) (Figure 1C). As shown in the previous panel, untreated cells (ligand-free AR) display essentially no AR ADP-ribosylation, while R1881 induces AR ADP-ribosylation (Figure 1C, lanes 2 and 3). By contrast, in comparison to R1881, HO-Flutamide induces only a near-background level AR ADP-ribosylation (Figure 1C, lanes 3 and 4). We used the same approach to analyze the ligand-dependence of AR T878A ADP-ribosylation. We found that treatment with HO-Flutamide resulted in ADP-ribosylation of the AR mutant to a level comparable with WT AR treated with R1881 (Figure 1C, lanes 3 and 7). Conformation-dependent phosphorylation [10] of Ser82 in the AR T878A mutant was induced slightly by HO-Flutamide (Figure 1C, lanes 5 and 7). From these data, we conclude that efficient ADP-ribosylation of AR by PARP7 requires an androgen-induced, agonist conformation of AR. The HO-Flutamide induction of ADP-ribosylation of AR T878A corroborates this view since the drug induces the agonist conformation in this mutant [12–14].

PARP7 nuclear localization is required for ADP-ribosylation of AR

The subcellular distribution of PARP7 is context specific. PARP7 localizes to the cytoplasm in ovarian cancer cells [15], and its anti-viral response function also occurs in the cytoplasm [16,17]. By contrast, PARP7 is primarily nuclear in other settings, including PCa cells (Bindesbøll et al., 2016; Gomez et al., 2018; Kamata et al., 2021; MacPherson et al., 2013; Roper et al., 2014). Because nuclear receptors such as AR shuttle between the nucleus and cytoplasm even when ligand-bound [18], PARP7 could encounter and ADP-ribosylate AR

in the cytoplasm, the nucleus, or both. We tested whether nuclear localization of PARP7 is required for AR ADP-ribosylation by using a series of nuclear transport signal mutations and fusions to control the steady state localization of PARP7 (Figure 2A). The series included mutation of the endogenous PARP7 NLS (“AAA”), fusion with the SV40 NLS (“NLS”), fusion of the c-Abl nuclear export signal (“NES”), and combinations of these signals. Tet-inducible cell lines expressing the PARP7 nuclear transport signal mutants and fusions were generated and analyzed by immunofluorescence microscopy. WT PARP7 is predominantly nuclear in the absence of androgen, and the nuclear:cytoplasmic (N:C) ratio is increased slightly by treating cells with R1881 (Figure 2B, C). Nuclear localization of PARP7 is dependent on its NLS since the AAA mutant accumulates in the cytoplasm (Figure 2B, C). The nuclear import defect of the PARP7 AAA mutant is rescued by the SV40 NLS (Figure 2B,C). Finally, PARP7 with an intact NLS can be forced into the cytoplasm with the c-Abl NES; the effect is more pronounced when combined with the AAA mutant (Figure 2B, C).

We analyzed the effect of PARP7 localization on AR modification by probing cell extracts for AR ADP-ribosylation and normalizing to the level of AR expression (Figure 2D). With this experimental setup, androgen induction of endogenous PARP7 results in a modest level of AR ADP-ribosylation which is increased by Tet induction of WT PARP7 (Figure 2D, compare lanes 2 and 4). Despite showing a mostly cytoplasmic distribution, the PARP7 AAA mutant was still capable of AR ADP-ribosylation (Figure 2D, compare lanes 4 and 6). The relatively small effect of mutating the PARP7 NLS on AR ADP-ribosylation suggests that a very low nuclear level of PARP7 is sufficient to modify AR in the nucleus. A stronger reduction in AR ADP-ribosylation was observed with the NES-AAA PARP7 mutant (Figure 2D, compare lanes 4 and 14). Thus, the level of AR ADP-ribosylation detected after co-expression with NES-AAA PARP7 was accounted for by endogenous PARP7 expression (Figure 2D, lanes 2 and 14). Overall, the data is consistent with a nuclear localization requirement for PARP7 to ADP-ribosylate AR. As expected, double label IF microscopy for PARP7 and AR shows that WT PARP7 and AR co-localize to the nucleus, except in cells expressing PARP7 NES-AAA and AR where the distribution is mutually exclusive in many cells (Figure 2E).

The ZF and the catalytic domain of PARP7 are required for regulation of AR-dependent gene transcription

PARP7 encodes a single Cys_3His_1-type ZF that other groups have shown is required for the transcription regulatory effect of PARP7 on liver X receptors [19] and aryl hydrocarbon receptor [20]. Although the function of the PARP7 ZF in these studies was not defined, the data raise the question of whether the ZF might be required generally for PARP7 to affect transcription factor activity. The ZF (amino acids 237-264) is encoded after the N-terminal domain, which is predicted to be mostly unstructured (Figure 3A). We engineered single cysteine-to-alanine substitutions to test if the PARP7 ZF is important for AR ADP-ribosylation and PARP7 effects on AR-dependent transcription, including ADP-ribosylation-dependent assembly of the AR-PARP9/DTX3L complex [7]. As controls, we also generated loss-of-function point mutations in the PARP7 catalytic domain, which allowed us to test for non-catalytic effects of PARP7 on the pathway. Using PC3-Flag-AR

cells with Tet-inducible WT and mutant forms of PARP7, we assayed expression of the *MYBPC1* gene by RT-qPCR since it shows a strong dependence on PARP7 for efficient induction by androgen and AR [7]. In this assay, the level of *MYBPC1* expression in the absence of Dox but the presence of R1881 includes the contribution by endogenous PARP7 (Figure 3B, No Dox, black bar). We found that mutation of the ZF (C243A, C251A) eliminated the PARP7 enhancement of androgen-induced *MYBPC1* transcription (Figure 3B). Similarly, amino acid substitutions that inactivate the catalytic function of PARP7 (H332A, H532A) rendered PARP7 inactive for androgen-induced *MYBPC1* transcription (Figure 3B). Using bead-immobilized AF1521 to pull-down ADP-ribosylated proteins from cell extracts, we found that the ZF mutations in PARP7 reduce AR ADP-ribosylation, but both mutants (C243A, C251A) retain catalytic activity as indicated by PARP7 auto-modification and pull-down on AF1521 beads (Figure 3C, lanes 5-8). Point mutations in the PARP7 catalytic domain eliminated AR ADP-ribosylation by ectopic PARP7, and extracts prepared from these mutants showed only a low level of AF1521 binding (Figure 3C, lanes 9-12). We next examined the effects of PARP7 point mutations on AR complex formation with PARP9/DTX3L, a reaction that reflects PARP7 ADP-ribosylation of AR and PARP9/DTX3L binding that uses the macrodomain reader function of PARP9 [7]. Compared to WT PARP7, cell lines expressing the ZF and catalytic domain mutants of PARP7 showed a low level of AR ADP-ribosylation and AR-PARP9/DTX3L formation that was ascribable to endogenous PARP7 induction by R1881 (Figure 3D, lanes 2, 5-8). Taken together, the data show that the ZF and the catalytic function of PARP7 are important for AR ADP-ribosylation, AR-PARP9/DTX3L complex formation, and enhancement of AR-dependent transcription of the *MYBPC1* gene.

ZF structure in PARP7 is dispensable for binding AR

ZF function is usually associated with nucleic acid binding, though there are examples of ZFs that mediate protein-protein interactions [21]. Our finding that substitutions C243A and C251A in PARP7 reduced AR ADP-ribosylation led us to investigate if the ZF plays a role in AR binding. We addressed this question by co-expression of PARP7 and AR in HEK293T cells and AR IP, and immunoblotting. We found that AR binding to PARP7 ZF mutant C243A and catalytic domain mutant H532A occurred at a level similar to that of PARP7 WT (Figure 4B). Binding assays performed with deletion mutants of PARP7 (Figure 4A) showed that the catalytic domain of PARP7 is sufficient for the interaction with AR (Figure 4C). PARP7 lacking a catalytic domain also bound to AR, and the interaction with the truncation mutant was unaffected by a ZF C243A substitution (Figure 4C). These data are consistent with a model that PARP7 uses multiple domains to contact AR, and binding is not dependent on ZF structure. We tested whether the PARP7 ZF is sufficient for binding AR using recombinant GST-ZF immobilized on beads and cell extracts that contain AR. AR did not bind the recombinant PARP7 ZF, nor did it bind the PARP7 ZF mutant C243A (Figure 4D). This result shows that the PARP7 ZF is not sufficient to bind AR, which together with the AR IP results with PARP7 ZF C243A (Figure 4B) suggests that the ZF is not used to bind AR. We acknowledge it is formally possible that PARP7 uses multiple sites to contact AR, including the ZF, and these are not revealed by the assay conditions. Nevertheless, the available data support the conclusion that the PARP7 ZF plays an important role in AR ADP-ribosylation that appears separable from protein binding and PARP7 catalytic activity.

Rescue of the nuclear localization defect caused by the PARP7 ZF mutant does not restore AR ADP-ribosylation

To explore other mechanisms through which the PARP7 ZF contributes to AR ADP-ribosylation, we considered the observation that the PARP7 ZF contributes to PARP7 nuclear localization [20,22]. Given that PARP7 requires nuclear localization to modify AR, mutations that reduce import would be predicted to impact PARP7 ADP-ribosylation of substrates in the nucleus. We first examined the localization of WT and various PARP7 mutants in PC3-Flag-AR cells by IF microscopy. The preferential nuclear localization observed for WT PARP7, particularly in the presence of R1881, was lost in the PARP7 C243A and C251A ZF mutants (Figure 5A, B). Both of the PARP7 catalytic domain mutants (H532A and Y564A) localized to the nucleus (Figure 5A,B), consistent with previous observations and emphasizing that PARP7 catalytic function is not a prerequisite for import [20,22,23].

With the goal of testing if the reduction in AR ADP-ribosylation observed with PARP ZF mutants can be explained by defective nuclear import, we designed a rescue experiment by appending the SV40 NLS to the PARP7 C243A mutant. We transfected WT, C243A, and NLS-C243A PARP7 (C243A PARP7 mutant fused to the SV40 NLS) into HEK293T cells, and after treatment with R1881, performed IF microscopy. When PARP7 distribution is plotted, it is clear that the PARP7 C243A mutant has a lower N:C ratio than PARP7 WT, and that the NLS-C243A PARP7 construct has an N:C value that is similar to WT PARP7. This result shows the SV40 NLS can rescue the nuclear localization defect of PARP7 C243A (Figure 5C,D). These constructs were then used to test whether rescue of nuclear localization was sufficient to restore AR ADP-ribosylation. Compared to WT PARP7, the PARP7 C243A mutant and the PARP7 NLS-C243A rescue construct showed only background levels of AR ADP-ribosylation (Figure 5E). Thus, although the ZF is important for efficient nuclear localization of PARP7, it also has a transport-independent function that is important for AR ADP-ribosylation inside the nucleus (Figure 5F).

Discussion

In this study, we extended our understanding of PARP7/AR signaling by exploring the features of AR and PARP7 that are necessary for AR ADP-ribosylation. Our data underscore the fact that the agonist conformation of AR is required for ADP-ribosylation by PARP7. The dependence on ligand binding for AR ADP-ribosylation is supported by the fact that the L860F mutation which disrupts androgen binding to AR [11] causes a substantial reduction in AR ADP-ribosylation. In HEK293T cells co-transfected with PARP7 and WT AR, we observed that androgen (agonist), but not HO-Flutamide (antagonist), treatment leads to ADP-ribosylation of AR. The result can be explained by the fact that compared to agonist binding, AR adopts a distinct conformation when bound to antagonists such as bicalutamide and HO-Flutamide [24– 26]. However, when the T878A substitution was introduced into the ligand binding domain, AR ADP-ribosylation became inducible by HO-Flutamide. This occurs because the T878A AR mutant can adopt an agonist conformation when antagonist is bound [12]. From these results, we conclude that the agonist conformation for AR is a key requirement for ADP-ribosylation by PARP7.

Another key finding from our study is the requirement of an intact PARP7 ZF domain for ADP-ribosylation of AR and concomitant assembly of the PARP9/DTX3L complex and regulation of AR-dependent transcription. The PARP7 ZF mutants C243A and C251A both retained auto-ADP-ribosylation activity as measured by AF1521 pull-down, indicating these mutant proteins are enzymatically active. Furthermore, the C243A PARP7 mutant co-immunoprecipitated with AR suggesting that ZF structure is dispensable for PARP7 binding to AR . Thus, neither the loss of catalytic activity nor loss of substrate binding seems to explain the ADP-ribosylation defect we observed using the PARP7 ZF mutants.

Additional data showed that in the context of full-length PARP7, an intact ZF domain was dispensable for AR binding, and GST pull-down assays suggested that the isolated ZF is not sufficient to bind AR. As shown by the Matthews group in other cell types [20,22], we found that the PARP7 ZF mutant displays a nuclear localization defect. Although nuclear localization of PARP7 is critical for AR ADP-ribosylation and can be disrupted by mutations within the ZF, we found that rescuing nuclear localization by fusing the SV40 NLS to the C243A PARP7 mutant did not restore ADP-ribosylation of AR. Thus, the ZF in PARP7 contributes to AR ADP-ribosylation by a mechanism that remains to be identified. The ZF could play a structural role that helps maintains overall PARP7 structure, and loss of this structural contribution results in a significant reduction in AR ADP-ribosylation. This could be considered an indirect contribution of the ZF for AR ADP-ribosylation. It is important to point out that PARP7 with ZF mutations still binds Af1521 beads, which we used as a surrogate for assessing PARP7 catalytic activity by auto-modification. Development and implementation of facile assays that directly measure PARP7 modification of substrate will enable a more rigorous exploration of this issue. Our binding data suggests that the ZF is not fundamentally important for binding AR, but a more definitive assessment of this issue will probably require analysis of protein structures.

In summary, this study and previous work [7] from our group has established that PARP7-mediated AR ADP-ribosylation is tightly coupled to ligand binding to AR. Indeed, in the absence of androgen, AR ADP-ribosylation is almost undetectable. The strict dependence of AR ADP-ribosylation on androgen treatment reflects the fact there are multiple androgen-sensitive features within the PARP7/AR signaling axis that are downstream of induction of the agonist conformation of AR (Figure 6). First, androgen binding to AR induces its translocation into the nucleus, which compartmentalizes the AR-PARP7 substrate-enzyme pair. PARP7 contains an NLS [22], and we and others have observed that PARP7 shows a preferential localization to the nucleus [9,20,22,27]. We showed in this study that nuclear localization of PARP7 is required for efficient AR ADP-ribosylation. Given that androgen binding to AR drives its import into the nucleus [28–30] where PARP7 localizes, it is logical that androgen-dependence of AR ADP-ribosylation is partly explained by the increased AR concentration in the nucleus. Second, *PARP7* is a direct AR target gene that is induced by androgen treatment [7,8]. Prior to androgen treatment, PARP7 levels in PCa cells detected by immunoblotting are extremely low, indicating that active AR signaling is required for PARP7 expression [9]. Third, PARP7 protein is stabilized by androgen signaling [9]. The androgen-dependent stabilization is a post-transcriptional mechanism that works in concert with *PARP7* mRNA induction to increase PARP7 protein level in cells. Critically, PARP7 protein stabilization leads to PARP7 accumulation in the nucleus with AR [9] .

Fourth, as demonstrated with the experiments using the AR L860F and T878A mutants, the agonist conformation of AR is required for AR ADP-ribosylation by PARP7. These features illustrate how the AR LBD can be used as a ligand-dependent molecular switch that controls both PARP7 biogenesis and utilization of AR as a substrate.

Materials and methods

Plasmid DNA

N-terminally 3xHA-tagged PARP7 WT, N-terminal region (amino acids: 1-456; NTR), and catalytic domain (amino acids: 457-657; CD) were cloned into the pKH3 vector. Site-directed mutagenesis (SDM) was conducted on pKH3/HA-PARP7 and pKH3/HA-PARP7 NTR to generate the following expression vectors: pKH3/HA-PARP7 C243A, pKH3/HA-PARP7 H532A, and pKH3/HA-PARP7 NTR-C243A. Additionally, SDM was used to introduce K41A/K42A/K43A substitutions in the TetON-HA-PARP7 lentiviral vector [9] to generate the TetON-HA-PARP7 AAA lentiviral vector. Annealed oligo cloning strategy was used to insert either the SV40 NLS (PKKKRKV) or c-Abl NES (EAINKLESNLRELQICPAT) between the HA tag and the PARP7 coding sequence to generate the following vectors: TetON-HA-PARP7 NLS, TetON-HA-PARP7 NES, TetON-HA-PARP7 NLS-AAA, TetON-HA-PARP7 NES-AAA, and pKH3/HA-PARP7 NLS-C243A. pCDNA3/Flag-AR was generated previously [31], and SDM was conducted on the vector to introduce the L860F substitution. pcDNA3/Flag-AR T878A was generated previously [28]. PARP7 ZF domain (amino acids: 232-269) was cloned into pGEX-vector for expression of the GST-fusion protein in *E. coli.* SDM was conducted on pGEX/GST-PARP7-ZF to introduce the C243A substitution in the zinc finger domain (pGEX/GST-PARP7-ZF-C243A)

Chemical Reagents

The following drugs were used in this study: R1881 (methyltrienolone; used at 2 nM) (PerkinElmer, Inc., Waltham, MA, USA) and hydroxyflutamide (HO-flutamide; used at 1 μM) (Sigma-Aldrich, St. Louis, MO, USA).

Antibodies

The following primary antibodies were used for this study: anti-AR (custom rabbit polyclonal against AR amino acid: 1-21 or amino acid: 656 to 669; prepared by Cocalico Biologicals, Inc., Stevens, PA, USA), anti-phospho-AR (Ser81) (rabbit polyclonal; Sigma-Aldrich), anti-HA (mouse monoclonal clone 16B12; Covance, Princeton, NJ, USA), anti-tubulin (mouse monoclonal clone TUB-1A2; Sigma-Aldrich), anti-DTX3L (custom rabbit polyclonal against DTX3L catalytic domain; Cocalico Biologicals, Inc.), and anti-PARP9 (custom rabbit polyclonal against PARP9 catalytic domain; Cocalico Biologicals, Inc.). The following secondary antibodies were used for immunoblotting: IRDye® 800-conjugated goat anti-mouse IgG (610-132-121; Rockland Immunochemicals, Inc., Limerick, PA, USA) and AlexaFluor® 680-conjugated donkey anti-rabbit IgG (A10043; Thermo Fisher Scientific, Waltham, MA, USA). For immunofluorescence microscopy, the following secondary antibodies were purchased from Jackson ImmunoResearch Laboratories,

Inc. (West Grove, PA, USA): Cy3-conjugated donkey anti-mouse (715-165-151), Cy5-conjugated donkey anti-rabbit (711-175-152), and AlexaFluor® 488-conjugated donkey anti-mouse (715-545-150) antibody.

Cell culture and transfections

PC3-Flag-AR and PC3-Flag-AR/TetON-HA-PARP7 (WT, C243A, C251A, H532A, and Y564A) cell lines were generated previously [9,32]. PC3-Flag-AR/TetON-HA-PARP7 NLS, PC3-Flag-AR/TetON-HA-PARP7 NES, PC3-Flag-AR/TetON-HA-PARP7 AAA, PC3-Flag-AR/TetON-HA-PARP7 NLS-AAA, and PC3-Flag-AR/TetON-HA-PARP7 NES-AAA cell lines were derived from PC3-Flag-AR via lentivirus transduction. All PC3 derived cells were grown in RPMI 1640 medium supplemented with 5% fetal bovine serum (SH30396.03HI; Cytiva, Marlborough, MA, USA) and 100 U/mL penicillin/streptomycin (Thermo Fisher Scientific). Puromycin (1 μg/mL) was added to culture medium to maintain selection for cell lines carrying the TetON vector. HEK293T cells were grown in DMEM/F12 (1:1) medium supplemented with 5% fetal bovine serum (Cytiva) and 100 U/mL penicillin/streptomycin (Thermo Fisher Scientific). All cells were grown at 37°C with 5% CO_2. Transient transfections into HEK293T cells were conducted using Lipofectamine 3000 (Thermo Fisher Scientific) according to manufacturer's protocol.

Detection of ADP-ribosylation

AF1521 is a macrodomain protein from the bacteria *Archaeoglobus fulgidus* that specifically binds to ADP-ribose [33] and was utilized in pull-down or as a direct blotting reagent for detection of ADP-ribosylation as described in [34]. Treated cells were lysed in 50 mM Tris-HCl pH 7.5, 150 mM NaCl, 0.5% Triton X-100 (v/v), 1 μg/mL aprotinin, 1 μg/mL leupeptin, 1 μg/mL pepstatin, 1 mM PMSF, and 1 mM DTT and incubated with magnetic glutathione beads (L00327; GenScript Biotech, Piscataway, NJ, USA) loaded with recombinant GST-tagged AF1521 for 2 to 4 hours at 4°C with rotation. Beads were washed five times with wash buffer (50 mM Tris-HCl pH 7.5, 150 mM NaCl, 0.1% Triton X-100 (v/v), and 1 mM DTT) and resuspended in 1× sample buffer for subsequent analysis by SDS-PAGE and immunoblotting. For direct blotting, recombinant GST-tagged tandem AF1521 was fluorescently labeled using IRDye® 800CW Protein Labeling Kit (LI-COR Biosciences, Lincoln, NE, USA). Prepared samples were run on SDS-PAGE, and proteins were immobilized on nitrocellulose membranes. After blocking for at least 1 h in milk solution (5% nonfat dry milk (w/v)/1× PBS with 0.15% Tween 20 (v/v) (1× PBST)), membranes were probed with the fluorescently-labeled AF1521 (4°C overnight) to detect ADP-ribosylated AR, and images were acquired using an Odyssey® CLx system (LI-COR Biosciences).

Co-immunoprecipitation

For co-immunoprecipitations from treated PC3-Flag-AR/TetON-HA-PARP7 cells, collected cell pellets were lysed in 50 mM Tris-HCl pH 7.5, 150 mM NaCl, 0.5% Triton X-100 (v/v), 1 μg/mL aprotinin, 1 μg/mL leupeptin, 1 μg/mL pepstatin, 1 mM PMSF, and 1 mM DTT. For co-immunoprecipitations from treated HEK293T cells, collected cell pellets were lysed in 20 mM HEPES pH 7.5, 200 mM NaCl, 0.5% NP-40, 1 μg/mL aprotinin, 1 μg/mL leupeptin, 1 μg/mL pepstatin, 1 mM PMSF, and 1 mM DTT. Clarified cell extract

were applied to magnetic anti-Flag M2 beads (M8823; Sigma-Aldrich) and incubated for 2 hours at 4°C with rotation. Beads were washed five times with the following wash buffers: 50 mM Tris-HCl pH 7.5, 150 mM NaCl, 0.1% Triton X-100 (v/v), and 1 mM DTT for co-immunoprecipitations from PC3-Flag-AR/TetON-HA-PARP7 cells, and 20 mM HEPES pH 7.5, 200 mM NaCl, 0.1% NP-40, and 1 mM DTT for co-immunoprecipitations from HEK293T cells. Washed beads were resuspended in 1× sample buffer and analyzed by SDS-PAGE and immunoblotting.

GST-PARP7-zinc finger pull-down

GST-tagged PARP7 zinc finger WT and C243A proteins were recombinantly expressed in *E. coli* and purified as described in [34] with the following modifications: 1) induction of GST-tagged proteins in *E. coli* was done in the presence of 50 μM $ZnCl_2$ in the culture medium, 2) lysis and elution buffers were supplemented with 1 μM $ZnCl_2$, and 3) after purification, GST-tagged proteins were dialyzed in 1× PBS, 1 μM $ZnCl_2$, and 2 mM DTT. Magnetic glutathione beads (L00327; GenScript Biotech) were loaded with the purified PARP7 zinc finger proteins, and subsequently incubated with extracts prepared from cell pellets lysed in 20 mM HEPES pH 7.5, 200 mM NaCl, 0.5% NP-40, 1 μg/mL aprotinin, 1 μg/mL leupeptin, 1 μg/mL pepstatin, 1 mM PMSF, 1 mM DTT, 100 U/mL RNase inhibitor, and 2 nM R1881. After 2 h incubation at 4°C with rotation, beads were washed four times with wash buffer (20 mM HEPES pH 7.5, 200 mM NaCl, 0.5% NP-40, 1 mM DTT, 100 U/mL RNase inhibitor, and 2 nM R1881) and resuspended in 1× sample buffer for analysis by SDS-PAGE and immunoblotting.

SDS-PAGE and immunoblotting

Samples were prepared in 1× sample buffer and analyzed by SDS-PAGE. After transfer, nitrocellulose membranes were blocked for 1 h in blocking solution (5% nonfat dry milk (w/v)/1× PBS with 0.15% Tween 20 (v/v) (1× PBST)), followed by primary and secondary antibody incubations. Membranes were washed five times between each step with 1× PBST. Fluorescent signal was detected using an Odyssey® CLx imaging system (LI-COR Biosciences), and quantification was done using the Image Studio Lite version 5.2.5 (LI-COR Biosciences).

Immunofluorescence microscopy

Coverslips were processed for immunofluorescence microscopy as described in [9]. Cells were seeded onto glass coverslips at least 48 h before processing. Treated cells were fixed with 3.75% formaldehyde/1× PBS for 15 minutes, permeabilized with 0.2% Triton X-100/1× PBS for five minutes, and blocked for 1 h at room temperature in blocking buffer (2% BSA (w/v)/1× PBS). Coverslips were incubated in primary antibody overnight at 4°C, and after washes, incubated in secondary antibody for 1 h at room temperature. Before mounting, washed coverslips were briefly incubated in DAPI to stain for nuclei, followed by a rinsing step with deioinized water. Coverslips were mounted on glass slides with VectaShield (Vector Laboratories, Burlingame, CA, USA). Images were acquired using a Nikon Eclipse Ni-U microscope (Nikon Instruments, Inc., Melville, NY, USA) equipped with a DS-Qi1Mc camera at 40× objective. All images were processed using Adobe Photoshop version 21.2.2 (Adobe Inc., San Jose, CA, USA) and Fiji ImageJ version 2.0.0.

HA-PARP7 cellular distribution was quantified as a ratio of nuclear (N) to cytoplasmic (C) signal as described previously [35]. N:C ratio was calculated from the background-corrected mean signal intensities of regions of interest outlined in the nucleus and the cytoplasm. At least 100 cells were quantified for each condition.

RT-qPCR

To isolate RNA, treated cells were processed using the RNeasy kit (QIAGEN, Hilden, Germany). cDNA was synthesized from 1 μg of isolated RNA using iScript cDNA synthesis kit (Bio-Rad Laboratories, Hercules, CA, USA). RT-qPCR was carried out using SensiMix™ SYBR® and Fluorescein kit (QT615-05; Bioline, London, United Kingdom). The following primers were used: *MYBPC1* (5′-GTCGCTCTCACATGGACTCC-3′ and 5′-AATGGTGGCACTGGTTCGAT-3′) and *GUS* (5′-CCGACTTCTCTGACAACCGACG-3′ and 5′-AGCCGACAAAATGCCGCAGACG-3’). Gene expression was normalized against the housekeeping gene *GUS*, and the mean and standard deviation were calculated from three biological replicates.

Statistical Analysis

All statistical analysis was conducted in GraphPad Prism version 9.0.1 software (GraphPad Software, San Diego, CA, USA). Statistical significance was determined using a one-way ANOVA with Tukey’s multiple comparison test as appropriate. All experiments in the study were performed two or more times with comparable results.

Funding

The work was supported by NCI award R01CA214872 to BMP, and a Robert R. Wagner Fellowship to TK at the University of Virginia.

Abbreviations

AR	androgen receptor
ZF	zinc finger
PCa	prostate cancer
NTR	amino terminal region
ADT	androgen deprivation therapy
LBD	ligand binding domain
NLS	nuclear localization signal
NES	nuclear export signal
R1881	methyltrienolone
N:C	nuclear:cytoplasmic

SDM	site directed mutagenesis

References

1. Bray F, Ferlay J, Soerjomataram I, Siegel RL, Torre LA and Jemal A (2018) Global cancer statistics 2018: GLOBOCAN estimates of incidence and mortality worldwide for 36 cancers in 185 countries. CA. Cancer J. Clin 68, 394–424. [PubMed: 30207593]
2. Robinson-Rechavi M, Garcia HE and Laudet V (2003) The nuclear receptor superfamily. J. Cell Sci, The Company of Biologists Ltd 116, 585–586. [PubMed: 12538758]
3. Tan ME, Li J, Xu HE, Melcher K and Yong E (2015) Androgen receptor: structure, role in prostate cancer and drug discovery. Acta Pharmacol. Sin 36, 3–23. [PubMed: 24909511]
4. Davey RA and Grossmann M (2016) Androgen Receptor Structure, Function and Biology: From Bench to Bedside. Clin. Biochem. Rev 37, 3–15. [PubMed: 27057074]
5. Gelmann EP (2002) Molecular Biology of the Androgen Receptor. J. Clin. Oncol 20, 3001–3015. [PubMed: 12089231]
6. Chism DD, Silva DD and Whang YE (2014) Mechanisms of acquired resistance to androgen receptor targeting drugs in castration-resistant prostate cancer. Expert Rev. Anticancer Ther, Taylor & Francis 14, 1369–1378. [PubMed: 24927631]
7. Yang C-S, Jividen K, Kamata T, Dworak N, Oostdyk L, Remlein B, Pourfarjam Y, Kim I-K, Du K-P, Abbas T, et al. (2021) Androgen signaling uses a writer and a reader of ADP-ribosylation to regulate protein complex assembly Nat. Commun, Nature Publishing Group 12, 2705. [PubMed: 33976187]
8. Bolton EC, So AY, Chaivorapol C, Haqq CM, Li H and Yamamoto KR (2007) Cell- and gene-specific regulation of primary target genes by the androgen receptor. Genes Amp Dev. 21, 2005–2017.
9. Kamata T, Yang C-S, Melhuish TA, Frierson HF Jr., Wotton D and Paschal BM (2021) Post-Transcriptional Regulation of PARP7 Protein Stability Is Controlled by Androgen Signaling. Cells, Multidisciplinary Digital Publishing Institute 10, 363. [PubMed: 33572475]
10. Gioeli D and Paschal BM (2012) Post-translational modification of the androgen receptor. Mol. Cell. Endocrinol 352, 70–78. [PubMed: 21820033]
11. Rajender S, Singh L and Thangaraj K (2007) L859F Mutation in Androgen Receptor Gene Results in Complete Loss of Androgen Binding to the Receptor. J. Androl 28, 772–776. [PubMed: 17522416]
12. Bohl CE, Gao W, Miller DD, Bell CE and Dalton JT (2005) Structural basis for antagonism and resistance of bicalutamide in prostate cancer. Proc. Natl. Acad. Sci 102, 6201–6206. [PubMed: 15833816]
13. Krasnov GS, Dmitriev AA, Sadritdinova AF, Volchenko NN, Slavnova EN, Danilova TV, Snezhkina AV, Melnikova NV, Fedorova MS, Lakunina VA, et al. (2015) Molecular genetic mechanisms of drug resistance in prostate cancer. Mol. Biol 49, 638–648.
14. Tian X, He Y and Zhou J (2015) Progress in antiandrogen design targeting hormone binding pocket to circumvent mutation based resistance. Front. Pharmacol., Frontiers 6.
15. Palavalli Parsons LH, Challa S, Gibson BA, Nandu T, Stokes MS, Huang D, Lea JS and Kraus WL (2021) Identification of PARP-7 substrates reveals a role for MARylation in microtubule control in ovarian cancer cells. eLife (Cole PA, Leung AK, Leung AK, and Matic I, eds.), eLife Sciences Publications, Ltd 10, e60481. [PubMed: 33475085]
16. Kozaki T, Komano J, Kanbayashi D, Takahama M, Misawa T, Satoh T, Takeuchi O, Kawai T, Shimizu S, Matsuura Y, et al. (2017) Mitochondrial damage elicits a TCDD-inducible poly(ADP-ribose) polymerase-mediated antiviral response. Proc. Natl. Acad. Sci 114, 2681–2686. [PubMed: 28213497]
17. Yamada T, Horimoto H, Kameyama T, Hayakawa S, Yamato H, Dazai M, Takada A, Kida H, Bott D, Zhou AC, et al. (2016) Constitutive aryl hydrocarbon receptor signaling constrains type I interferon–mediated antiviral innate defense. Nat. Immunol 17, 687–694. [PubMed: 27089381]
18. Black BE and Paschal BM (2004) Intranuclear organization and function of the androgen receptor. Trends Endocrinol. Metab 15, 411–417. [PubMed: 15519887]

19. Bindesbøll C, Tan S, Bott D, Cho T, Tamblyn L, MacPherson L, Grønning-Wang L, Nebb HI and Matthews J (2016) TCDD-inducible poly-ADP-ribose polymerase (TIPARP/PARP7) mono-ADP-ribosylates and co-activates liver X receptors. Biochem. J 473, 899–910. [PubMed: 26814197]
20. MacPherson L, Tamblyn L, Rajendra S, Bralha F, McPherson JP and Matthews J (2013) 2,3,7,8-Tetrachlorodibenzo-p-dioxin poly(ADP-ribose) polymerase (TiPARP, ARTD14) is a mono-ADP-ribosyltransferase and repressor of aryl hydrocarbon receptor transactivation. Nucleic Acids Res. 41, 1604–1621. [PubMed: 23275542]
21. Brayer KJ and Segal DJ (2008) Keep Your Fingers Off My DNA: Protein–Protein Interactions Mediated by C2H2 Zinc Finger Domains. Cell Biochem. Biophys 50, 111–131. [PubMed: 18253864]
22. Gomez A, Bindesbøll C, Satheesh SV, Grimaldi G, Hutin D, MacPherson L, Ahmed S, Tamblyn L, Cho T, Nebb HI, et al. (2018) Characterization of TCDD-inducible poly-ADP-ribose polymerase (TIPARP/ARTD14) catalytic activity. Biochem. J 475, 3827–3846. [PubMed: 30373764]
23. Zhang L, Cao J, Dong L and Lin H (2020) TiPARP forms nuclear condensates to degrade HIF-1α and suppress tumorigenesis. Proc. Natl. Acad. Sci, National Academy of Sciences.
24. Helsen C, Broeck T. V. den, Voet A, Prekovic S, Poppel HV, Joniau S and Claessens F (2014) Androgen receptor antagonists for prostate cancer therapy. Endocr. Relat. Cancer, Bioscientifica Ltd 21, T105–T118.
25. Hodgson MC, Shen HC, Hollenberg AN and Balk SP (2008) Structural basis for nuclear receptor corepressor recruitment by antagonist-liganded androgen receptor. Mol. Cancer Ther 7, 3187–3194. [PubMed: 18852122]
26. Sakkiah S, Kusko R, Pan B, Guo W, Ge W, Tong W and Hong H (2018) Structural Changes Due to Antagonist Binding in Ligand Binding Pocket of Androgen Receptor Elucidated Through Molecular Dynamics Simulations. Front. Pharmacol., Frontiers 9.
27. Roper SJ, Chrysanthou S, Senner CE, Sienerth A, Gnan S, Murray A, Masutani M, Latos P and Hemberger M (2014) ADP-ribosyltransferases Parp1 and Parp7 safeguard pluripotency of ES cells. Nucleic Acids Res. 42, 8914–8927. [PubMed: 25034692]
28. Ni L, Llewellyn R, Kesler CT, Kelley JB, Spencer A, Snow CJ, Shank L and Paschal BM (2013) Androgen Induces a Switch from Cytoplasmic Retention to Nuclear Import of the Androgen Receptor. Mol. Cell. Biol., American Society for Microbiology Journals 33, 4766–4778.
29. Kaku N, Matsuda K, Tsujimura A and Kawata M (2008) Characterization of Nuclear Import of the Domain-Specific Androgen Receptor in Association with the Importin α/β and Ran-Guanosine 5'-Triphosphate Systems. Endocrinology 149, 3960–3969. [PubMed: 18420738]
30. Zhou ZX, Sar M, Simental JA, Lane MV and Wilson EM (1994) A ligand-dependent bipartite nuclear targeting signal in the human androgen receptor. Requirement for the DNA-binding domain and modulation by NH2-terminal and carboxyl-terminal sequences. J. Biol. Chem 269, 13115–13123. [PubMed: 8175737]
31. Gioeli D, Ficarro SB, Kwiek JJ, Aaronson D, Hancock M, Catling AD, White FM, Christian RE, Settlage RE, Shabanowitz J, et al. (2002) Androgen Receptor Phosphorylation: Regulation and Identification of the Phosphorylation Sites. J. Biol. Chem 277, 29304–29314. [PubMed: 12015328]
32. Jividen K, Kedzierska KZ, Yang C-S, Szlachta K, Ratan A and Paschal BM (2018) Genomic analysis of DNA repair genes and androgen signaling in prostate cancer. BMC Cancer 18, 960. [PubMed: 30305041]
33. Karras GI, Kustatscher G, Buhecha HR, Allen MD, Pugieux C, Sait F, Bycroft M and Ladurner AG (2005) The *macro* domain is an ADP-ribose binding module. EMBO J. 24, 1911–1920. [PubMed: 15902274]
34. Kamata T, Yang C-S, Jividen K, Spencer A, Dworak N, Oostdyk LT and Paschal BM (2019) Detection of ADP-Ribosylation of the Androgen Receptor Using the Recombinant Macrodomain AF1521 from Archaeoglobus fulgidus. In Nuclear Receptors: Methods and Experimental Protocols (Badr MZ, ed.), pp 107–124, Springer New York, New York, NY.
35. Kelley JB and Paschal BM (2019) Fluorescence-based quantification of nucleocytoplasmic transport. Methods 157, 106–114. [PubMed: 30419335]

36. Erdős G and Dosztányi Z (2020) Analyzing Protein Disorder with IUPred2A. Curr. Protoc. Bioinforma 70, e99.

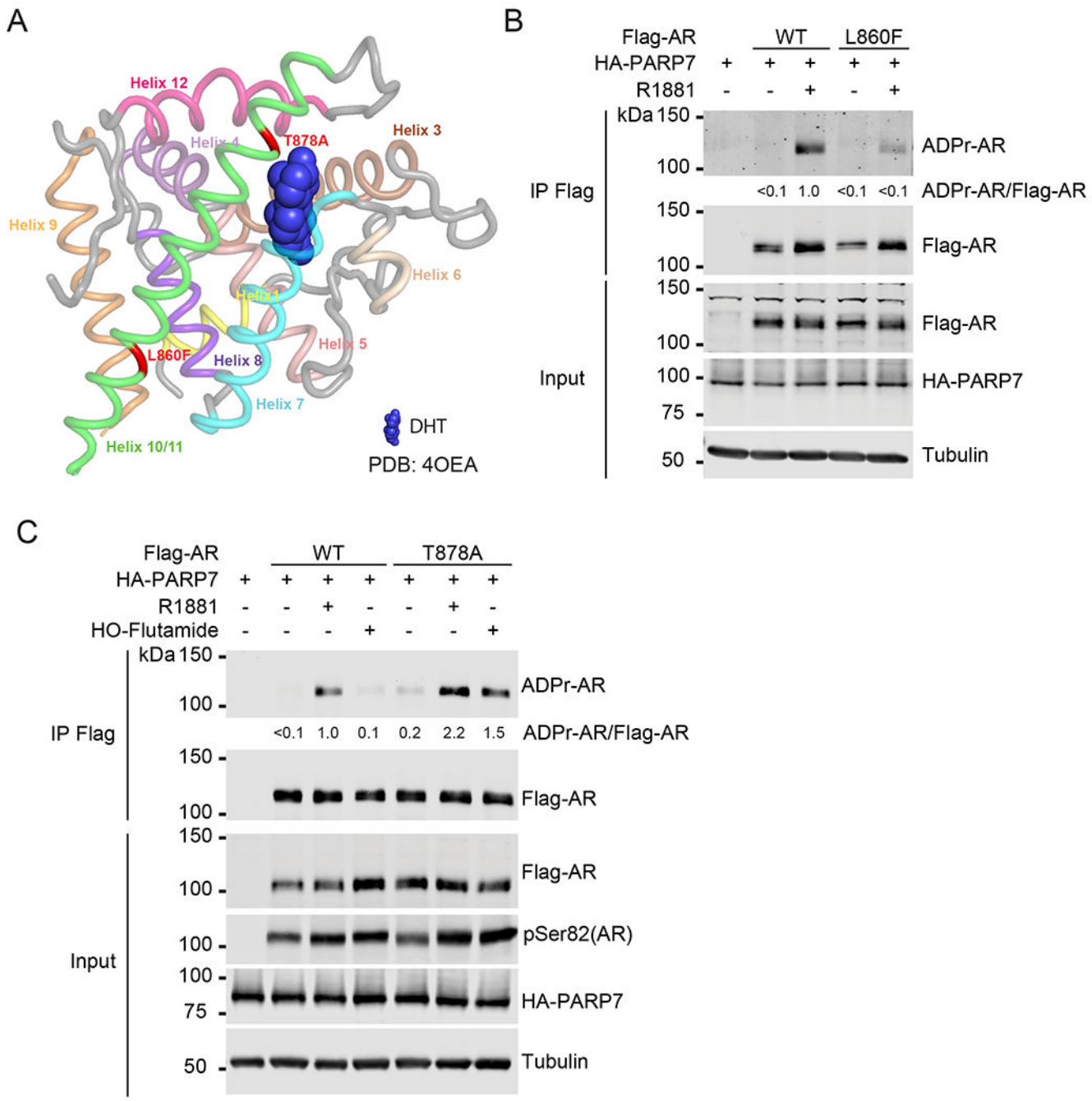

Figure 1.

The agonist conformation of AR is critical for mono-ADP-ribosylation by PARP7. (**A**) Structure of the human AR LBD (amino acids 671-920) bound to the agonist, dihydrotestosterone (DHT; blue) (PDB: 4OEA). The model is a smoothed backbone trace with helices shown in different colors. Amino acid substitutions T878A and L860F are indicated in red. (**B**) HEK293T cells were transfected with HA-PARP7 and Flag-AR (WT and L860F). After 24 h, transfected cells were treated with R1881 for 8 h. Flag-AR was immunoprecipitated and analyzed for ADP-ribosylation. ADP-ribosylated AR (ADPr-AR)

was quantified as a ratio of ADPr-AR to AR. Ratios are displayed relative to the WT + R1881 lane (set to 1.0). (**C**) HEK293T cells were transfected with HA-PARP7 and Flag-AR (WT and T878A). After 24 h, cells were treated with R1881 and hydroxyflutamide (HO-Flutamide) for 8 h. Flag-AR was immunoprecipitated and analyzed for AR ADP-ribosylation.

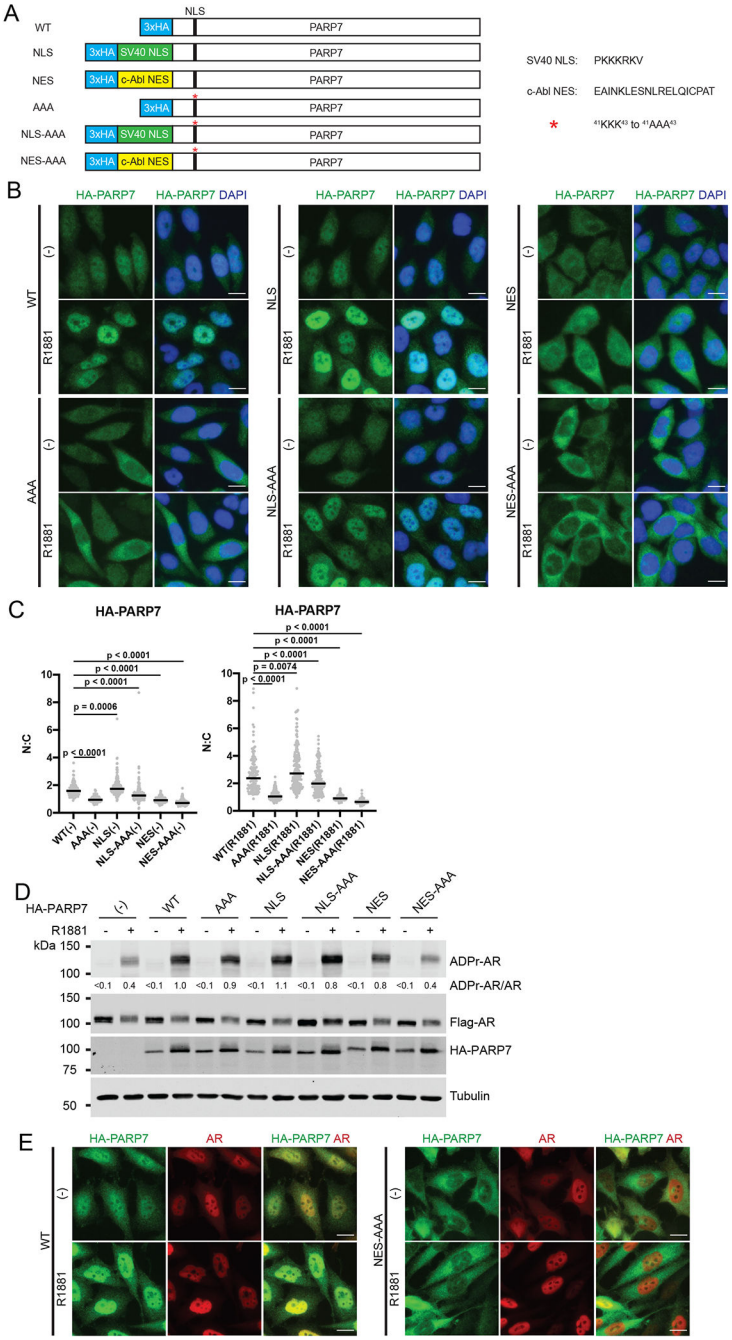

Figure 2.

Nuclear localization of PARP7 is required for ADP-ribosylation of AR (**A**) Schematic of PARP7 constructs. Triple alanine (AAA) subsitutions were made in the endogenous NLS of PARP7 to generate the AAA PARP7 mutant. SV40 NLS and c-Abl NES fusions were created with WT and AAA PARP7, as indicated. (**B**) HA-PARP7 WT and mutant proteins were induced in PC3-Flag-AR cells by doxycycline addition (2 μg/mL, 24 h), and further treated with R1881 for 6 h. Cells were processed for immunofluorescence microscopy. Scale bar = 5 μm. (**C**) Quantification of PARP7 subcellular localization using

immunofluorescence images. HA- Nuclear (N) and cytoplasmic (C) PARP7 was quantified and plotted as a ratio, using data from vehicle (left) and R1881-treated (right) groups. At least 100 cells were quantified per condition, and median N:C ratio (black line) is indicated on the plots. One-way ANOVA with Tukey's multiple comparison test was conducted to determine statistical significance. (**D**) PC3-Flag-AR cells expressing HA-PARP7 WT or mutant were induced with doxycycline and treated with R1881 as in panel (B) and analyzed for AR ADP-ribosylation by immunoblotting. ADPr-AR was quantified as a ratio of ADPr-AR to AR. Ratios are displayed relative to the WT + R1881 lane (set to 1.0). (**E**) PC3-Flag-AR cells expressing WT or NES-AAA PARP7 were induced with doxycycline and treated with R1881 as in (B). Treated cells were co-stained for HA-PARP7 and Flag-AR for immunofluroescence microscopy. Scale bar = 5 μm.

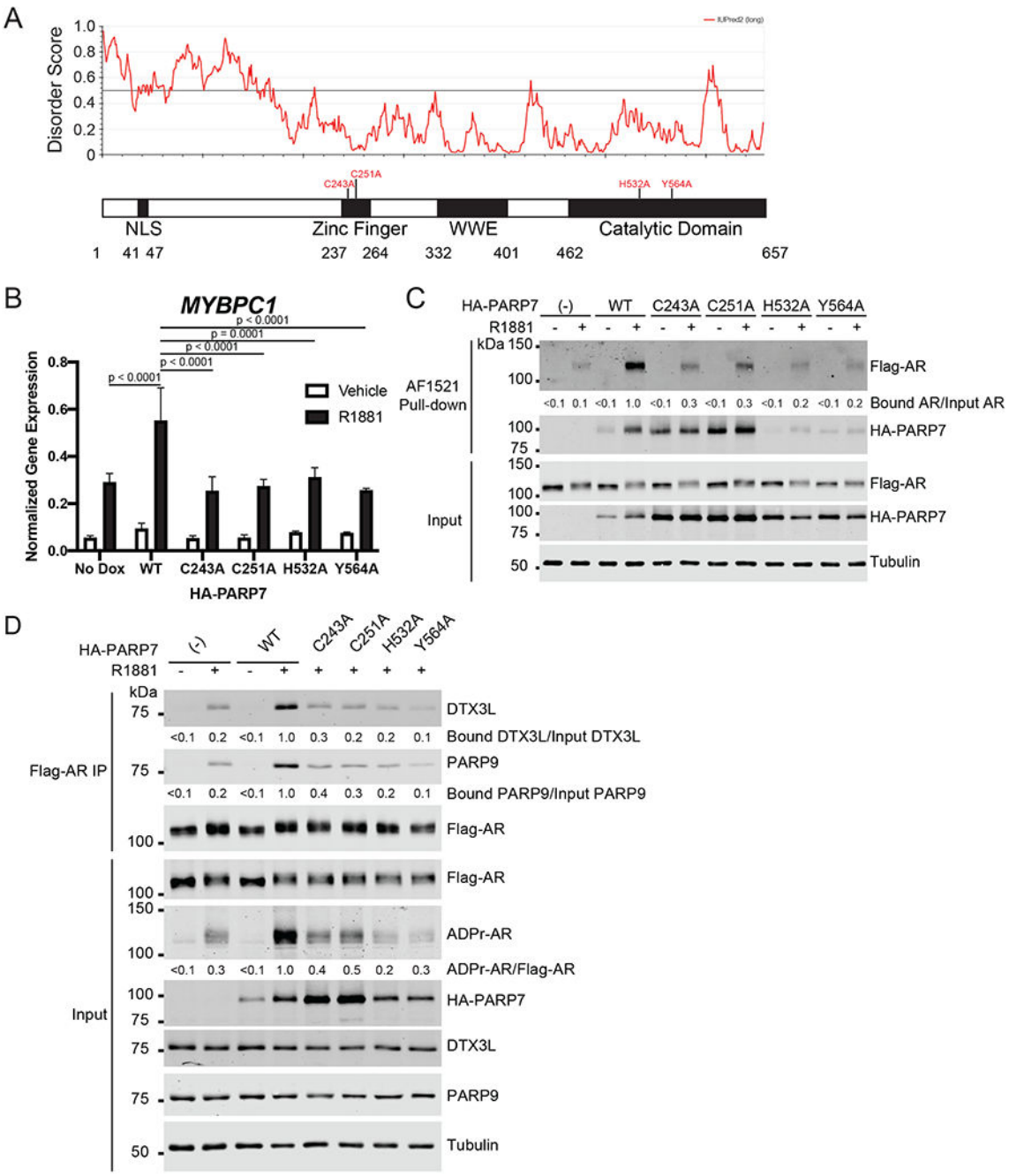

Figure 3.

The ZF and catalytic domains of PARP7 are required for AR ADP-ribosylation, assembly of the PARP9/DTX3L complex, and regulation of AR-dependent gene transcription. (**A**) Domain architecture of PARP7 and amino acid substitutions (red) used in the study. Prediction of disorder regions by IUPred2A [36] is also plotted. NLS, nuclear localization signal; WWE, tryptophan-tryptophan-glutamate domain. (**B**) Effect of PARP7 on AR-dependent transcription of the *MYBPC1* gene. PARP7 WT and mutants (C243A, C251A, H532A, and Y564A) were induced in PC3-Flag-AR cells by doxycycline (2 μg/mL) for

24 hours. An untreated sample served as an uninduced control (No Dox). Cells were then androgen treated (2 nM R1881) for 9 hours, and RNA isolated and analyzed for gene expression of *MYBPC1*. Gene expression was normalized to the housekeeping gene *GUS*. Plots represent mean ± SD from three biological replicates. One-way ANOVA with Tukey's multiple comparison test was conducted to determine statistical significance. Higher expression levels of the PARP7 mutants is routinely observed and likely reflects the longer protein half-lives relative to the WT PARP7, which we showed previously [9]. (**C**) PC3-Flag-AR cells expressing HA-PARP7 WT and mutants were induced with doxycycline similar to the previous panel. Cells were subsequently treated with R1881 for 6 h, and AR and HA-PARP7 ADP-ribosylation was analyzed by AF1521 pull-down. Bound AR was quantified as a ratio of bound AR to input AR. Ratios are displayed relative to the WT + R1881 lane (set to 1.0). (**D**) PC3-Flag-AR cells expressing PARP7 WT or mutant were treated as in (**C**). Flag-AR was immunoprecipitated and analyzed for DTX3L and PARP9 complex assembly. Bound DTX3L and PARP9 was quantified similar to C). ADPr-AR was quantified as a ratio of ADPr-AR to input AR. Ratios are displayed relative to the WT + R1881 lane (set to 1.0).

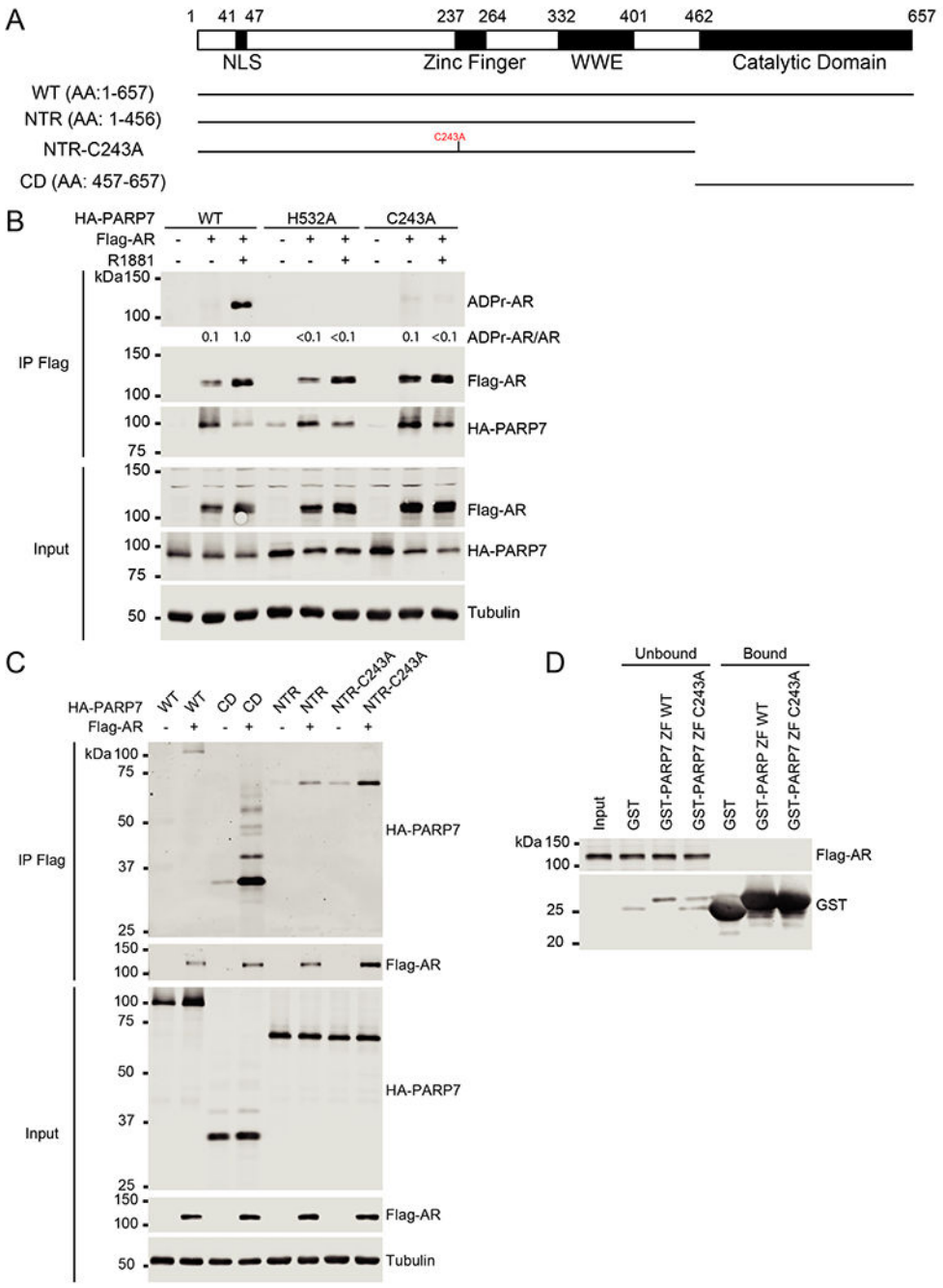

Figure 4.

ZF structure is not required for PARP7 to bind AR. (**A**) Schematic of PARP7 deletion mutants used for co-immunopreciptiation. NTR, N-terminal region; CD, catalytic domain. (**B**) HEK293T cells were transfected with Flag-AR and with HA-PARP7 WT, H532A, and C243A mutants. After 24 h, cells were treated with R1881 for 8 h. Flag-AR was immunoprecipitated and analyzed for AR ADP-ribosylation and interaction with HA-PARP7. ADP-ribosylated AR (ADPr-AR) was quantified as a ratio of ADPr-AR to AR. Ratios are displayed relative to the WT + R1881 lane (set to 1.0). (**C**) HEK293T cells were

transfected with the indicated HA-PARP7 construct either alone or with Flag-AR. After 24 h, Flag-AR was immunoprecipitated and analyzed for HA-PARP7 interaction. (**D**) Extract from PC3-Flag-AR cells treated with R1881 for 3 h was incubated with GST-fused PARP7 zinc finger domain (WT and C243A) immobilized on glutathione beads before analysis by SDS-PAGE and immunoblotting.

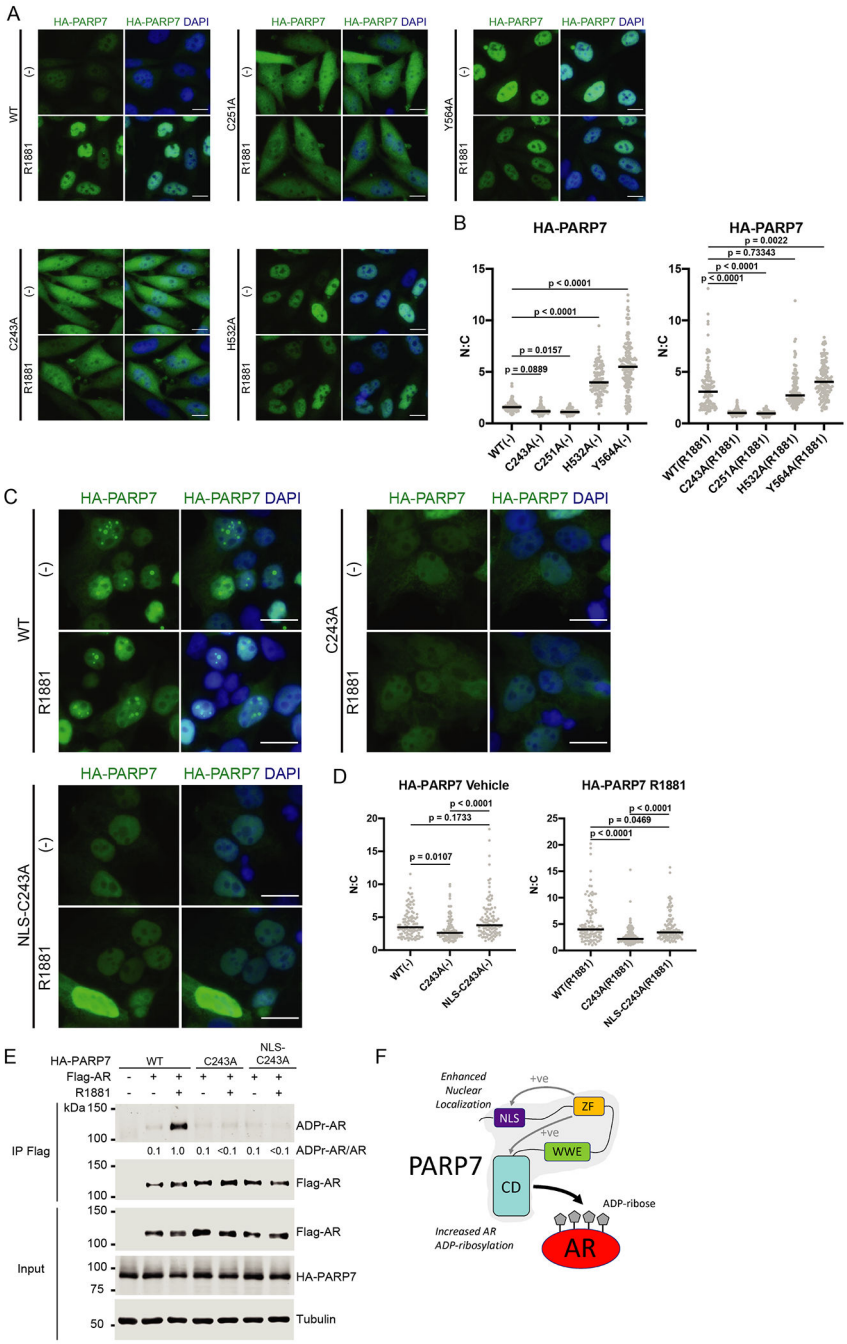

Figure 5.

The PARP7 ZF modulates nuclear import and has a second function related to AR-ADP-ribosylation. (**A**) PC3-Flag-AR cells expressing HA-PARP7 WT or mutant were induced with doxycycline and treated with R1881 similar to Fig 2B. Treated cells were processed for immunofluorescence microscopy. Scale bar = 5 μm. (**B**) Quantification of panel (**A**). Distribution of HA-PARP7 was quantified as a ratio of nuclear (N) and cytoplasmic (C) signals for vehicle- (left) and R1881-treated (right) groups . At least 100 cells were quantified for each condition, and median N:C ratio (black line) is indicated on the plots.

One-way ANOVA with Tukey's multiple comparison test was conducted to determine statistical significance. (**C**) HEK293T cells were transfected with Flag-AR along with HA-PARP7 WT, C243A, and NLS-C243A mutants (SV40 NLS fused to C243A PARP7). After 24 h, cells were treated with R1881 for 8 h and processed for immunofluorescence microscopy. Scale bar = 5 μm. (**D**) Quantification of (**C**). Distribution of HA-PARP7 was quantified as a ratio of nuclear (N) and cytoplasmic (C) signals for vehicle (left) and R1881-treated (right) groups similar to (**B**). At least 100 cells were quantified for each condition, and median N:C ratio (black line) is indicated on the plots. One-way ANOVA with Tukey's multiple comparison test was conducted to determine statistical significance. (**E**) HEK293T cells were transfected with Flag-AR along with HA-PARP7 WT, C243A, and NLS-C243A mutants and treated as in (**C**). Flag-AR was immunoprecipitated analyzed for AR ADP-ribosylation. ADP-ribosylated AR (ADPr-AR) was quantified as a ratio of ADPr-AR to AR. Ratios are displayed relative to the WT + R1881 lane (set to 1.0). (**F**) Cartoon showing how the ZF contributes to PARP7 activity. The ZF enhances (+ve, positive) steady state nuclear localization, possibly by promoting recognition of the NLS by the import machinery, or through an effect based on nuclear retention. The ZF contribution to AR ADP-ribosylation is separable from the ZF effect on PARP7 nuclear localization.

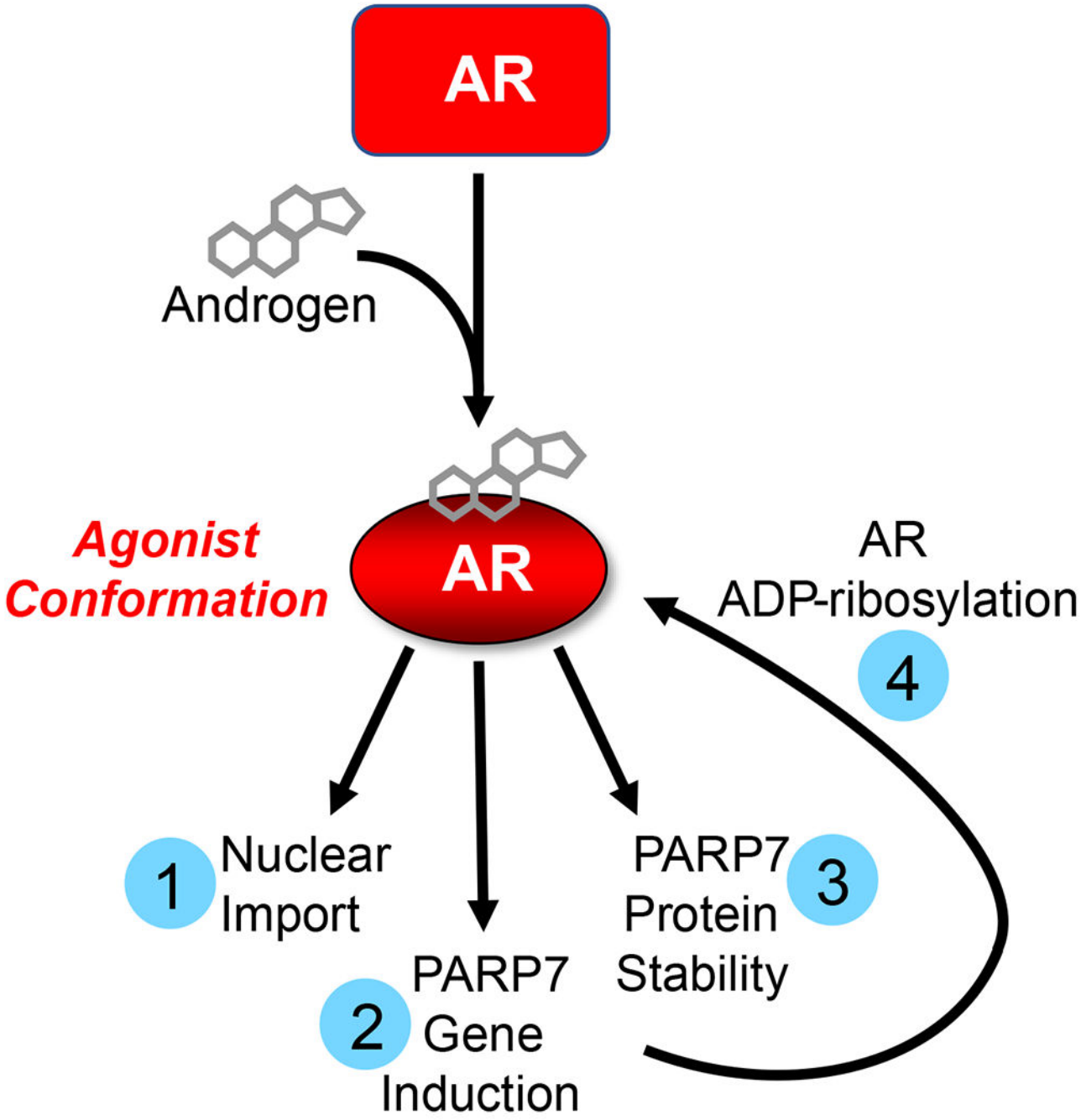

Figure 6.

Androgen induction of the agonist conformation of AR and integration with PARP7. The graphic summarizes the data presented in this study and previous work from our group [7,9,34]. Androgen binding induces an agonist conformation in AR that supports AR ADP-ribosylation through four events: (i) androgen induction of AR import into the nucleus; (ii) AR-mediated induction of PARP7 transcription; (iii) AR-dependent transcription that

results in PARP7 protein stabilization and its accumulation in the nucleus; and (iv) PARP7 ADP-ribosylation of the agonist conformation of AR.